Acta Crystallographica Section B
Structural Science
ISSN 0108-7681

Single-crystal-to-single-crystal $E \rightarrow Z$ isomerization of tiglic acid in a supramolecular framework

Shao-Liang Zheng, Marc Messerschmidt and Philip Coppens*

Department of Chemistry, State University of New York at Buffalo, Buffalo, NY 14260-3000, USA

Correspondence e-mail: coppens@buffalo.edu, chem9994@buffalo.edu

Received 20 February 2007
Accepted 13 April 2007

The single-crystal-to-single-crystal $E \rightarrow Z$ photoisomerization of tiglic acid (2,3-dimethylacrylic acid) occurs in the supramolecular crystals CECR–HTA·2MeOH·1.5H_2O (1) (where HTA = tiglic acid, CECR = *C*-ethylcalix[4]resorcinarene) with the preservation of the crystal lattice, indicating the 'scaffolding effect' of the molecular framework, which holds the crystal together notwithstanding the change in shape of the embedded guest molecules. A photostationary state is reached at a concentration of *ca* 30% of the *Z* isomers. A kinetic analysis shows the $Z \rightarrow E$ back-reaction to proceed with a larger rate constant than the $E \rightarrow Z$ isomerization.

1. Introduction

In parallel with the dramatically increased potential of single-crystal diffraction methods, our knowledge of photochemical reactions in crystals has advanced considerably beyond the early pioneering work of Schmidt and coworkers (Cohen *et al.*, 1964). However, topotactic (single-crystal-to-single-crystal) reactions, which proceed with the retention of the crystal lattice and can therefore be studied in detail by diffraction methods, are the exception in neat or co-crystals of photoreacting species, as emphasized in a number of review articles (see, for example, Keating & Garcia-Garibay, 1998). Topotactic reactions are mainly limited to intramolecular cyclizations (Leibovitch *et al.*, 1997, 1998; Hosomi *et al.*, 2000; Lavy *et al.*, 2004; Turowska-Tyrk *et al.*, 2006), in which the molecular migration is minimal, and to dimerization and polymerization reactions, including [2 + 2] (Tanaka *et al.*, 1999, 2000; Turowska-Tyrk, 2003; Gao *et al.*, 2004; Friščić *et al.*, 2005) and [4 + 4] cycloadditions (Turowska-Tyrk & Trzop, 2003; Kaftory *et al.*, 2005).

Topotactic reactions also occur in much more complex solids in which the reacting center is shielded by a large mantel of inert molecular components. Many physiological reactions are triggered by photochemical processes including the *cis–trans* ($Z \rightarrow E$) isomerization of rhodopsin (Tsukamoto *et al.*, 2005) and the *trans–cis* ($E \rightarrow Z$) isomerization of photoactive yellow protein (Rajagopal *et al.*, 2004; Getzoff *et al.*, 2003). As pointed out in recent publications (see, for example, Amirsakis *et al.*, 2003; Toda & Bishop, 2004; Ananchenko *et al.*, 2006; Halder & Kepert, 2006; Zouev *et al.*, 2006; Coppens *et al.*, 2006), supramolecular host–guest solids dramatically increase the possibility of monitoring photochemically induced processes in the periodic solid state. By embedding photoactive species in an inert host lattice, three-dimensional periodicity can often be retained as a reaction proceeds. We show here that this strategy can be applied to $E \rightarrow Z$ reactions.

E/*Z* photoisomerizations in neat crystals are generally not topotactic (Keating & Garcia-Garibay, 1998; Kaupp, 2002)

Table 1
Experimental details.

	200 K	90 K
Crystal data		
Chemical formula	$C_{43}H_{59}O_{13.50}$	$C_{43}H_{59}O_{13.50}$
M_r	791.90	791.90
Cell setting, space group	Triclinic, $P\bar{1}$	Triclinic, $P\bar{1}$
Temperature (K)	200 (2)	90 (2)
a, b, c (Å)	11.3467 (14), 14.1629 (18), 14.8100 (19)	11.2958 (2), 14.0716 (3), 14.7200 (3)
α, β, γ (°)	108.886 (4), 109.437 (4), 92.483 (4)	108.7556 (8), 108.6284 (7), 93.0151 (7)
V (Å^3)	2092.9 (5)	2067.74 (7)
Z	2	2
D_x (Mg m^{-3})	1.257	1.272
Radiation type	Mo $K\alpha$	Mo $K\alpha$
μ (mm^{-1})	0.09	0.09
Crystal form, colour	Block, pale yellow	Block, pale yellow
Crystal size (mm)	0.14 × 0.10 × 0.08	0.14 × 0.10 × 0.08
Data collection		
Diffractometer	CCD area detector	CCD area detector
Data collection method	φ and ω scans	φ and ω scans
Absorption correction	Empirical (using intensity measurements)	Empirical (using intensity measurements)
T_{min}	0.987	0.987
T_{max}	0.993	0.993
No. of measured, independent and observed reflections	14 548, 7230, 4698	27 003, 7281, 6643
Criterion for observed reflections	$I > 2\sigma(I)$	$I > 2\sigma(I)$
R_{int}	0.036	0.016
θ_{max} (°)	25.0	25.0
Refinement		
Refinement on	F^2	F^2
$R[F^2 > 2\sigma(F^2)]$, $wR(F^2)$, S	0.072, 0.219, 1.06	0.040, 0.113, 1.07
No. of reflections	7230	7281
No. of parameters	523	559
H-atom treatment	Constrained to parent site	Mixture of independent and constrained refinement
Weighting scheme	$w = 1/[\sigma^2(F_o^2) + (0.1228P)^2 + 0.8046P]$, where $P = (F_o^2 + 2F_c^2)/3$	$w = 1/[\sigma^2(F_o^2) + (0.0601P)^2 + 1.1813P]$, where $P = (F_o^2 + 2F_c^2)/3$
$(\Delta/\sigma)_{max}$	< 0.0001	< 0.0001
$\Delta\rho_{max}$, $\Delta\rho_{min}$ (e Å^{-3})	0.78, −0.44	0.66, −0.39

and [2 + 2] dimerization or polymerization, which occurs when C═C bonds are oriented parallel in sufficiently close proximity (Cohen *et al.*, 1964; Scheffer *et al.*, 1987; Ananchenko *et al.*, 2006), can be a complication. We show here that $E \rightarrow Z$ photoisomerization of HTA proceed in the supramolecular solid, CECR–HTA·2MeOH·1.5H_2O (1) (where HTA = tiglic acid, CECR = *C*-ethylcalix[4]resorcinarene, Figs. 1 and 2), to a photostationary state of ∼ 30% of the *Z* isomer under preservation of the integrity of the crystal lattice. Although $E \rightarrow Z$ and $Z \rightarrow E$ isomerizations in the solid state have been described before (see, for example, Arad-Yellin *et al.*, 1979; Kinbara *et al.*, 1996; Tanaka *et al.*, 2003; Naturajan *et al.*, 2006), this is the first report on a system with ordered reactant molecules in which crystallinity is fully preserved during the *trans–cis* isomerization.

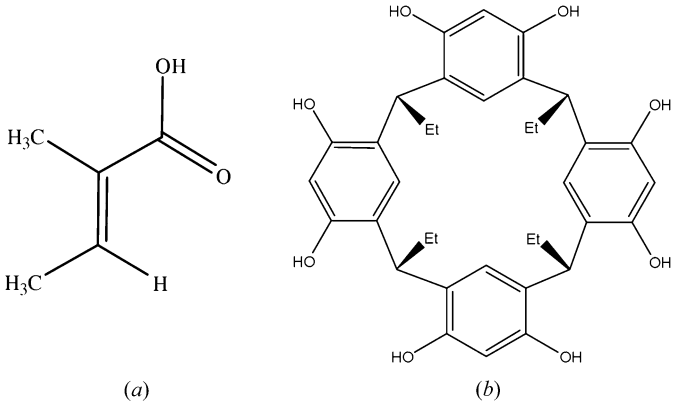

(*a*) (*b*)

Figure 1
The structure of (*a*) HTA and (*b*) CECR.

2. Experimental

2.1. Synthesis

A methanol solution (3 ml) of HTA (0.05 mmol) was added slowly to a stirred methanol solution (5 ml) of CECR (0.05 mmol) at 323 K for 30 min. Pale yellow crystals were obtained after 2 weeks through slow evaporation at room temperature (yield: 62%).

2.2. X-ray crystallography

Data on (1) were collected at 200 and 90 K on a Bruker APEX II CCD diffractometer installed at a rotating anode source (Mo $K\alpha$ radiation, λ = 0.71073 Å) and equipped with an Oxford Cryosystems nitrogen flow apparatus. 0.3° scans in ω were used with the detector positioned at $2\theta = 20°$. Data integration up to 0.82 Å resolution was carried out using *SAINT*, Version 7.34 (Bruker AXS, 2006) with reflection spot-size optimization. Absorption corrections were made with the program *SADABS* (Bruker AXS, 2006). The crystal was subsequently exposed stepwise at 90 K to 325 nm light from a 48 mW He/Cd laser for accumulated periods of 1, 3, 6 and 12 h. It was rotated around the φ axis during irradiation. X-ray data were collected at 90 K 1 h after the completion of each step of the irradiation. The parent structure was solved by direct methods and refined by least-squares against F^2 using *SHELXS*97 and *SHELXL*97 (Sheldrick, 2000). For the parent structure, non-H atoms were refined anisotropically, the hydroxy H atoms were located in difference maps after which the riding model was applied. Other H atoms were positioned at idealized positions and refined in the same way. For the structures after irradiation, all non-H atoms of the product

Table 2
Selected experimental details after 1, 3, 6 and 12 h exposure.

	1 h exposure	3 h exposure	6 h exposure	12 h exposure
a, b, c (Å)	11.2954 (2), 14.0883 (3), 14.7549 (3)	11.2902 (4), 14.1299 (6), 14.7991 (6)	11.2988 (6), 14.1506 (8), 14.8012 (9)	11.3096 (12), 14.1748 (16), 14.8116 (17)
α, β, γ (°)	108.6380 (5), 108.8086 (5), 92.9259 (6)	108.5839 (13), 109.2657 (12), 92.5600 (13)	108.5606 (18), 109.4747 (18), 92.4244 (19)	108.570 (3), 109.632 (4), 92.276 (4)
V (Å^3)	2074.74 (7)	2082.65 (14)	2085.7 (2)	2091.2 (4)
D_x (Mg m^{-3})	1.268	1.263	1.261	1.258
No. of measured, independent and observed reflections	16 740, 7308, 6443	16 761, 7340, 5019	17 425, 7340, 4384	15 054, 7351, 3760
R_{int}	0.014	0.032	0.041	0.049
$R[F^2 > 2\sigma(F^2)]$, $wR(F^2)$, S	0.042, 0.119, 1.09	0.056, 0.157, 1.17	0.063, 0.176, 1.21	0.071, 0.194, 1.20
No. of reflections	7308	7340	7340	7351
No. of parameters	581	581	581	581
$(\Delta/\sigma)_{max}$	0.001	0.003	< 0.0001	0.002
$\Delta\rho_{max}$, $\Delta\rho_{min}$ (e Å^{-3})	0.58, −0.32	0.48, −0.41	0.46, −0.38	0.49, −0.41
Conversion percentage	12.8 (4)	26.1 (6)	28.7 (7)	30.3 (9)

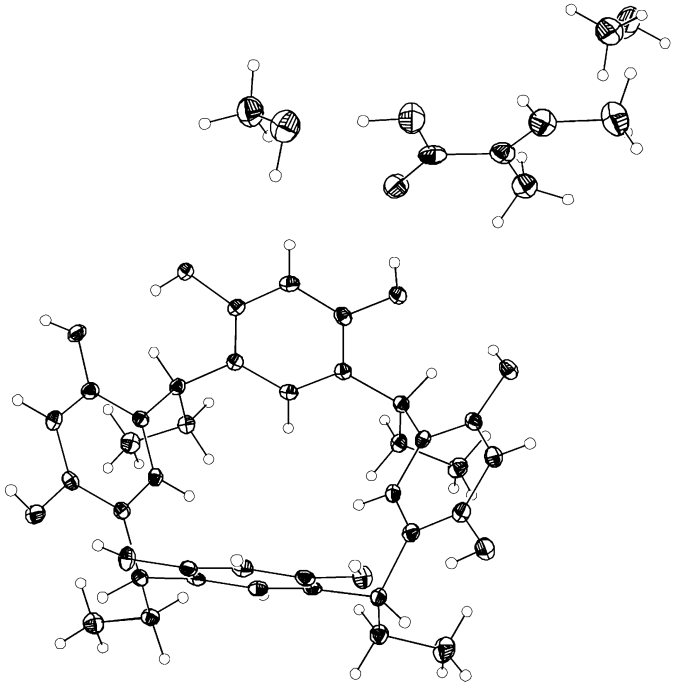

Figure 2
Perspective views showing the HTA, CECR and methanol molecules in (1) with 50% probability displacement ellipsoids. The disordered water molecules in (1) have been removed for clarity.

were located in difference-Fourier maps, calculated with coefficients F_0(*exposed*) − F_0(*pre-exposure*), and then refined with restraints on the product molecule's bond lengths and constraints of the atomic displacement parameters to the corresponding values of the reactant molecule (SADI and EADP instructions of *SHELXL*97). The riding model was used for the H atoms. The percentage of the reactant in the crystal was treated as a variable in the refinements. Crystal data as well as details of data collection and refinement are summarized in Tables 1 and 2,[1] while hydrogen bond distances and angles at 90 K are listed in Table 3. Difference-Fourier maps were produced with *XDFOUR* of the *XD*2006 program package (Volkov *et al.*, 2006); the *ORTEP* diagrams were plotted with *SHELXL*97 and *Weblab Viewer Pro*4.0 (Molecular Simulations Inc., 1997) was used for the molecular and packing diagrams.

3. Results and discussion

The CECR molecules in (1) adopt the bowl-shaped (*r-cis-cis-cis*) conformation with a C_s symmetric (Fig. S1 of the supplementary material) arrangement of the intramolecular hydrogen bonds along the upper rim [90 K: O···O = 2.712 (2)–2.932 (2) Å, Table 3]. Adjacent CECRs are connected in an up-and-down fashion by intermolecular hydrogen bonds [O···O = 2.675 (2)–2.746 (2) Å], to form wave-like layers parallel to the (010) plane with the deep bowl-shaped cavities (Figs. 3 and S2 of the supplementary material). Adjacent hydrogen-bonded layers are juxtaposed along the *b* axis such that the bowl-shaped cavities combine into channels along the *a* axis with a 10.8 × 4.2 Å effective cross-section, accounting for 34.8% of the crystal volume (Spek, 2003). In each unit cell, a fully ordered HTA molecule and its symmetry-related equivalent are embedded in the channel. Two fully ordered methanol molecules are hydrogen bonded to the hydroxyl O atoms [O···O = 2.727 (2) Å, Fig. 3] of adjacent CECR molecules and the carboxylic O atoms of the adjacent HTA [O···O = 2.591 (2) Å]. Some disordered waters are clathrated in each cavity to fill the remaining void.

The external shape of the crystal and its colour are essentially unaffected by the exposure (Fig. S3 of the supplementary material). The difference-Fourier maps after 3 h exposure clearly show light-induced peaks corresponding to a conversion of part of the molecules to the *Z* configuration (Figs. 4 and 5), and to shifts in the position of the reacted molecule, which effectively reduces the repulsion of the methyl group of the *Z* molecule by the channel wall. The dihedral angle between the *Z* molecule plane (C42*B*—C43*B*—C44*B*, label *B* indicates the atom in the converted complex) and that of the *E* molecule

[1] Supplementary data for this paper are available from the IUCr electronic archives (Reference: BK5051). Services for accessing these data are described at the back of the journal.

Table 3
Hydrogen-bond distances (Å) and angles (°) at 90 K.

D—H···A	$d_{D\cdots A}$ (Å)	∠DHA (°)	D—H···A	$d_{D\cdots A}$ (Å)	∠DHA (°)
O1—H1O···O8	2.757 (2)	164 (2)	O6—H6O···O7	2.712 (2)	174 (2)
O2—H2O···O9	2.756 (2)	169 (2)	O7—H7O···O1^{i}	2.675 (2)	162 (2)
O3—H3O···O6^{ii}	2.746 (2)	142 (2)	O10—H10O···O1S	2.591 (2)	173 (2)
O3—H3O···O2	2.932 (2)	123 (2)	O1S—H1S···O2S^{iii}	2.709 (2)	167.8
O4—H4O···O5	2.745 (2)	165 (2)	O2S—H2S···O4^{iv}	2.727 (2)	173.4
O5—H5O···O3^{v}	2.739 (2)	171 (2)			

Symmetry codes: (i) $-x-1, -y+1, -z$; (ii) $x+1, y, z$; (iii) $x-1, y, z$; (iv) $-x+1, -y+1, -z+1$; (v) $-x, -y+1, -z+1$.

Table 4
Volume of the channels in (1) at 90 K at different lengths of exposure.

Exposure time (h)	0	1	3	6	12
Crystal volume (Å^3)	2069.4	2074.7	2082.7	2085.7	2091.2
Volume (Å^3) of the channels (% of crystal volume)	718.9 (34.8%)	723.9 (34.9%)	730.1 (35.3%)	732.9 (35.1%)	731.0 (35.0%)
Cavity volume per HTA molecule (Å^3)	170.9	171.6	176.2	178.0	178.4

(C42—C43—C44) is 8.6 (1)°, while the distance between the C44*B* atom and the *E* molecule plane (C42—C43—C44) is 0.562 (2) Å. The least-squares refinement indicates that after 3 h exposure 26.1 (3)% of the HTA molecules have converted to the *Z* form (Figs. 3 and 6; Table S1 of the supplementary material). In the course of the reaction the product HTA molecules undergo a shift and a reorientation, as do the methanol molecules (Figs. 3 and S4 of the supplementary material). Such a rearrangement of the guest molecules has been observed in other solid-state reactions (Weiss *et al.*, 1993; Keating & Garcia-Garibay, 1998; Naturajan *et al.*, 2006). Only a very small expansion of the unit cell (Table S1 of the supplementary material) occurs, but the cavity size per HTA increases steadily during the irradiation at the expense of the volume occupied by the solvent molecules (Table 4).

The conversion percentage of HTA in the crystal as a function of the length of irradiation, as determined in the least-squares refinement, is presented in Fig. 5. The curve is well fitted by the exponential equation $y = 0.303\,(0) - 0.305\,(7)\ \exp[-t/1.67\,(10)]$ ($R = 0.997$), indicating reversible first-order kinetics, as observed in other photochemical solid-state reactions (Keating & Garcia-Garibay, 1998; Turowska-Tyrk, 2004). The application of standard kinetic expressions (Atkins & de Paula, 2001) leads to relative rate constants of $k(E \rightarrow Z) = 0.18\,(5)h^{-1}$ and $k(Z \rightarrow E) = 0.42\,(5)h^{-1}$, indicating that the return to the *E* state is more rapid than the initial photoinduced change, which is reasonable as the framework structure must be optimized for the *E* guest conformation. The absolute values of the rate constants given here depend on the incident photon flux and the oscillator strength of the photoinduced transition to the reactive (π^*) excited state. Parallel TDDFT (time-dependent density functional theory) calculations show the corresponding energy gaps and oscillator strengths to be practically identical for the *E* and *Z* isomers (Zheng *et al.*, 2007).

It has been argued that for solid-state reactions requiring significant molecular motions or involving changes in molecular shape, the initiation occurs at defects or surface sites in the crystal and that the crystal lattice is destroyed when conversion percentages exceed 5–10%, even though the external shape of the crystals may be perfectly retained (Kaupp, 2002). This is clearly not the case in the system studied here. Even though the conversion percentage is quite large and both the shape of the guest and its position are affected by the *E*/*Z* photoisomerization, unit-cell changes are minor (∼1%) (Tables 1 and 2, and S1 of the supplementary material), confirming that the host molecules form a stable scaffolding that preserves the crystal. It may be noted that an unequal composition of the reactants in the photostationary state is quite common for solid solid-state photoreactions. It is to be attributed to steric restrictions in the crystal which affect the rela-

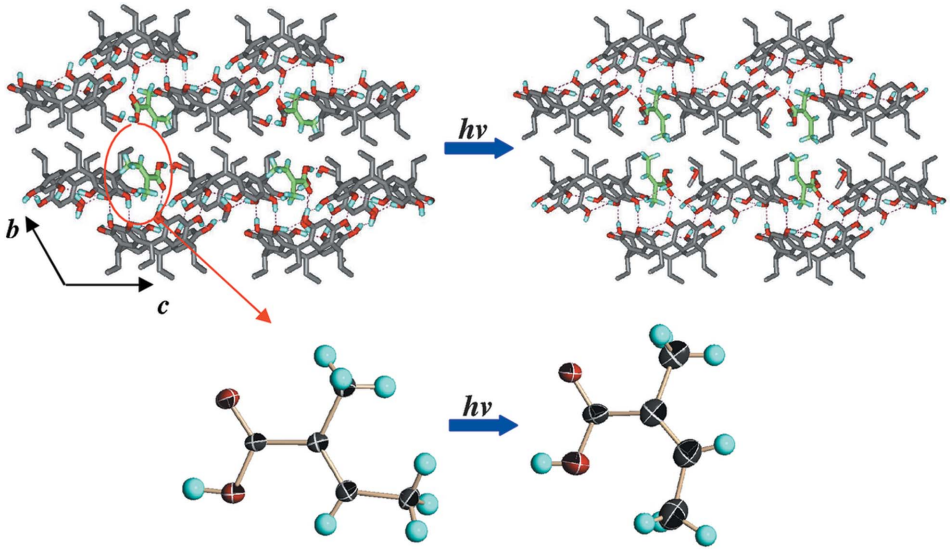

Figure 3
Three-dimensional supramolecular architecture of (1) viewed along the *a*-axis direction (top) and perspective views showing 50% probability displacement ellipsoids of the *E* molecule before exposure and the *Z* molecules after 3 h exposure (bottom).

tive rates of conversion (Keating & Garcia-Garibay, 1998; Takagi & Shichi, 2003).

Finally, the average of the principal mean square-atomic displacements $\langle U_{eq} \rangle$ over all the O/C atoms of the host molecules (CECR) increases with the length of irradiation (Fig. 6). Although all the photoreaction experiments were strictly carried out at 90 K, and the conversion percentage does increases only slightly after the first 3 h of exposure, the U_{eq} values continue to increase, suggesting crystal decay that is mainly due to irradiation rather than isomerization.

4. Conclusions

We conclude that the $E \rightarrow Z$ photoisomerization can proceed in supramolecular solids with the preservation of crystal integrity. The rate constants of the forward and back reactions, and therefore the composition of the photostationary state, are affected by the solid-state environment. In the tiglic acid–CECR complex studied the return of the Z molecules to the 'native' E state is faster than the opposite process, which may be interpreted as the *trans* (E) molecules fitting better in the original framework. A parallel study of chloroacrylic acid–CECR in which different photostationary states are reached starting from slightly different E and the Z-containing supramolecular frameworks has been reported elsewhere (Zheng *et al.*, 2007).

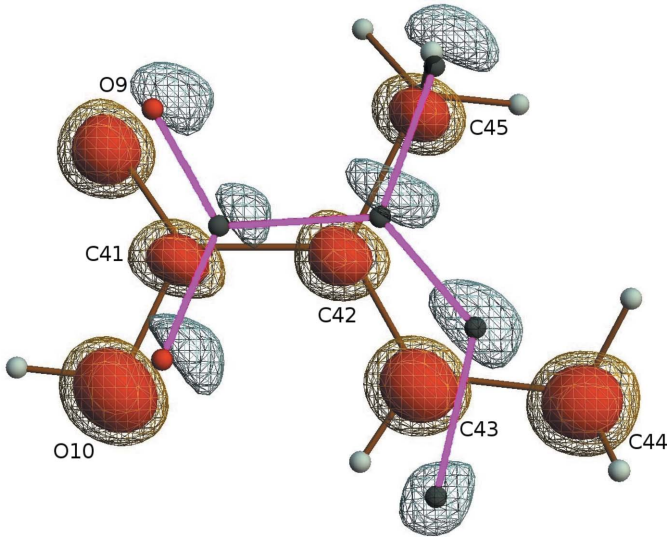

Figure 4
The difference-Fourier map of the HTA in (1) after 3 h exposure. Blue: 2.0 e Å^{-3}; light blue: 1.0 e Å^{-3}; orange: −1.0 e Å^{-3}; red: −2.0 e Å^{-3}.

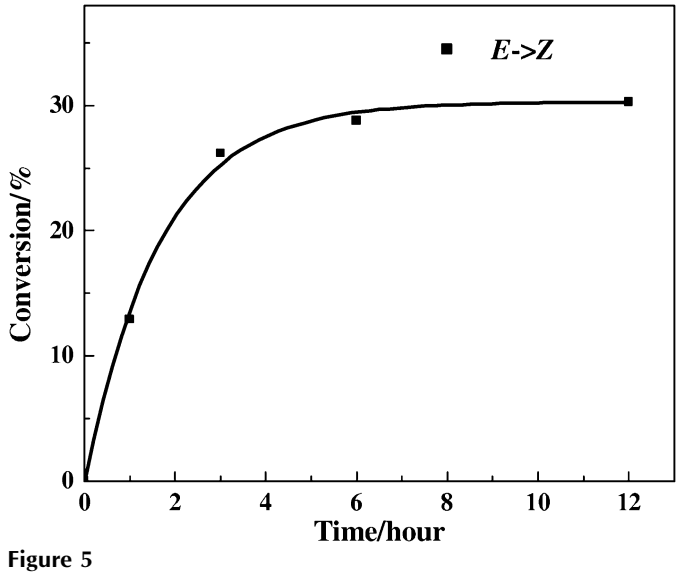

Figure 5
The photo-induced $E \rightarrow Z$ conversion radio of HTA in (1).

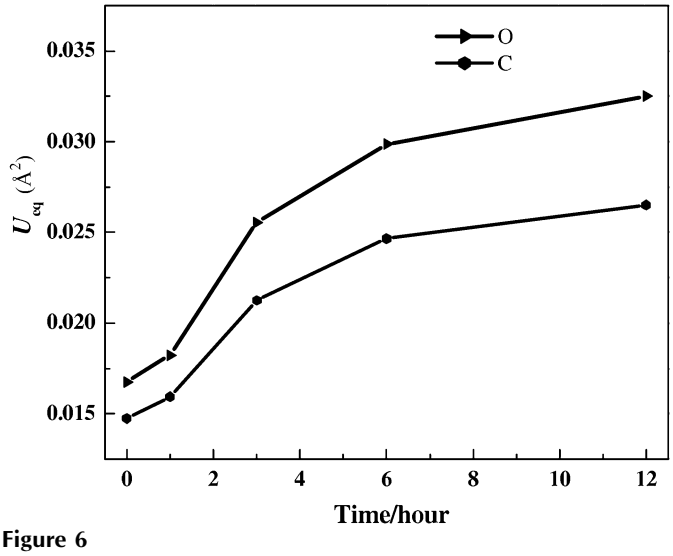

Figure 6
The relationship between U_{eq} averaged over the O/C atoms of the host molecules (CECR) and the length of the irradiation.

This work was supported by the Petroleum Research Fund of the American Chemical Society (PRF#43594-AC4) and the National Science Foundation (CHE0236317).

References

Amirsakis, D. G., Elizarov, A. M., Garcia-Garibay, M. A., Glink, P. T., Stoddart, J. F., White, A. J. & Williams, D. J. (2003). *Angew. Chem. Int. Ed.* **42**, 1126–1132.
Ananchenko, G. S., Udachin, K. A., Ripmeester, J. A., Perrier, T. & Coleman, A. W. (2006). *Chem. Eur. J.* **12**, 2441–2447.
Arad-Yellin, R., Brunie, S., Green, B. S., Knossow, M. & Tsoucaris, G. (1979). *J. Am. Chem. Soc.* **101**, 7529–7537.
Atkins, P. & de Paula, J. (2001). *Physical Chemistry*, 7th Ed, p. 876. New Jersey: W. H. Freeman.
Bruker AXS (2006). *SMART* and *SAINTPLUS*. Bruker AXS, Madison, Wisconsin.
Cohen, M. D., Schmidt, G. M. J. & Sonntag, F. I. (1964). *J. Chem. Soc.* pp. 2000–2013.
Coppens, P., Zheng, S.-L., Gembicky, M., Messerschmidt, M. & Dominiak, P. M. (2006). *CrystEngComm*, **8**, 735–741.
Friščić, T. & MacGillivray, L. R. (2005). *Z. Kristallogr.* **220**, 351–363.
Gao, X., Friščić, T. & MacGillivray, L. R. (2004). *Angew. Chem. Int. Ed.* **43**, 232–236.
Getzoff, E. D., Gutwin, K. N. & Genick, U. K. (2003). *Nature Struct. Biol.* **10**, 663–668.
Halder, G. & Kepert, C. (2006). *Aust. J. Chem.* **59**, 597–604.
Hosomi, H., Ohba, S., Tanaka, K. & Toda, F. (2000). *J. Am. Chem. Soc.* **122**, 1818–1819.

Kaftory, M., Shteiman, V., Lavy, T., Scheffer, J. R., Yang, J. & Enkelmann, V. (2005). *Eur. J. Org. Chem.* pp. 847–853.
Kaupp, G. (2002). *Curr. Opin. Solid State Mater. Sci.* **6**, 131–138.
Keating, A. E. & Garcia-Garibay, M. A. (1998). *Photochemical Solid-to-Solid Reactions*, edited by V. Ramamurthy & K. S. Schanze. New York: Marcel Dekker, Inc.
Kinbara, K., Kai, A., Maekawa, Y., Hashimoto, Y., Naruse, S., Hasegawa, M. & Saigo, K. (1996). *Mol. Cryst. Liq. Cryst.* **276**, 141–151.
Lavy, T., Sheynin, Y. & Kaftory, M. (2004). *Eur. J. Org. Chem.* pp. 4802–4808.
Leibovitch, M., Olovsson, G., Scheffer, J. R. & Trotter, J. (1997). *J. Am. Chem. Soc.* **119**, 1462–1463.
Leibovitch, M., Olovsson, G., Scheffer, J. R. & Trotter J. (1998). *J. Am. Chem. Soc.* **120**, 12755–12769.
Molecular Simulations Inc. (1997). *Weblab Viewer Pro*4.0. Molecular Simulations Inc., San Diego, California, USA.
Naturajan, A., Mague, J. T., Venkatesan, K., Arai, T. & Ramamurthy, V. (2006). *J. Org. Chem.* **71**, 1055–1059.
Rajagopal, S., Schmidt, M., Anderson, S., Ihee, H. & Moffat, K. (2004). *Acta Cryst.* D**60**, 860–871.
Scheffer, J. R., Garcia-Garibay, M. & Nalamasu, O. (1987). *Organic Photochemistry*, edited by A. Padwa, Vol. 8, pp. 319–324. New York: Marcel Dekker.
Sheldrick, G. M. (2000). *SHELXTL*6.10. Bruker Analytical Instrumentation, Madison, Wisconsin, USA.
Spek, A. L. (2003). *PLATON*. Utrecht University, The Netherlands.
Takagi, K. & Shichi, T. (2003). *Solid State and Surface Photochemistry*, edited by V. Ramamurthy & K. S. Schanze. New York: Marcel Dekker, Inc.
Tanaka, K., Hiratsuka, T., Ohba, S., Naimi-Jamai, M. R. & Kaup, G. (2003). *J. Phys. Org. Chem.* **16**, 905–912.
Tanaka, K., Toda, F., Mochizuki, E., Yasui, N., Kai, Y., Miyahara, I. & Hirotsu, K. (1999). *Angew. Chem. Int. Ed.* **38**, 3523–3526.
Tanaka, K., Toda, F., Mochizuki, E., Yasui, N., Kai, Y., Miyahara, I. & Hirotsu, K. (2000). *Tetrahedron*, **56**, 6853–6865.
Toda, F. & Bishop, B. (2004). *Separations and Reactions in Organic Supramolecular Chemistry: Perspectives in Supramolecular Chemistry*, Vol. 8. New York: John Wiley and Sons.
Tsukamoto, H., Terakita, A. & Shichida, Y. (2005). *Proc. Natl. Acad. Sci.* **102**, 6303–6308.
Turowska-Tyrk, I. (2003). *Acta Cryst.* B**59**, 670–675.
Turowska-Tyrk, I. (2004). *J. Phys. Org. Chem.* **17**, 837–847.
Turowska-Tyrk, I. & Trzop, E. (2003). *Acta Cryst.* B**59**, 779–786.
Turowska-Tyrk, I., Trzop, E., Scheffer, J. R. & Chen, S. (2006). *Acta Cryst.* B**62**, 128–134.
Volkov, A., Macchi, P., Farrugia, L. J., Gatti, C., Mallinson, P., Richter, T. & Koritsanszky, T. (2006). *XD*2006; see http://xd.chem.buffalo.edu.
Weiss, R. G., Ramamurthy, V. & Hammond, G. (1993). *Acc. Chem. Res.* **26**, 530–536.
Zheng, S.-L., Messerschmidt, M. & Coppens, P. (2007). *Chem. Commun.* pp. 2735–2737.
Zouev, I., Lavy, T. & Kaftory, M. (2006). *Eur. J. Org. Chem.* 4164–4169.